

# Germanium-on-Carborundum Surface Phonon-Polariton Infrared Metamaterial

Bo Qiang, Alexander M. Dubrovkin,\* Harish N. S. Krishnamoorthy, Qian Wang, Nikolay I. Zheludev,\* and Qi Jie Wang\*

Surface phonon-polaritons in thin layers of high-index dielectric structures are emerging as promising excitations for exploitation in high-density photonic devices. Here, a mid-infrared phononic–dielectric metamaterial, a 2D periodic array of germanium discs on silicon carbide (carborundum) is demonstrated. It is shown that the metamaterial can support sharp resonances at the free space wavelength that is at least ten times larger than lattice parameter of the array. With germanium discs of thickness 120 nm and diameter 1  $\mu\text{m}$ , a metamaterial resonance at the wavelength of 11  $\mu\text{m}$  is observed. A blueshift of the resonant frequency observed upon increase of the disk size is related to the anomalous dispersion of surface polaritons at germanium carborundum interface. It is argued that such surface phonon-polariton metamaterial is a promising platform for applications where enhanced homogeneity of optical response is required, such as imaging, holography, and cloaking.

In the past two decades, metamaterials have proven themselves as a powerful platform for achieving and engineering unusual electromagnetic properties of matter such as magnetic response in high-frequency regime,<sup>[1]</sup> negative refraction,<sup>[2]</sup> asymmetric propagation of light,<sup>[3]</sup> toroidal dipolar response,<sup>[4]</sup> and many others. However, the deployment of metamaterials in particular

application such as imaging, cloaking, and high-resolution synthetic holography is hampered by size of the metamolecules (unit cells) that are typically only a few times smaller than the wavelength of light at which resonant properties of metamaterial can be observed. Although in the microwave domain metamaterials lattice parameter orders or magnitude smaller than the resonant wavelength have been demonstrated,<sup>[5,6]</sup> in conventional optical and infrared metamaterial the unit cell-to-wavelength ratio is typically in the range from one-fourth to one-half. While the effective medium approximation<sup>[7–9]</sup> is often used to describe overall properties of such metamaterials, their electromagnetic homogeneity is still far away from that of natural solids where the crystal lattice parameter to wavelength ratio is typically

$10^{-3}$ – $10^{-4}$ . In this paper, we show that the use of surface phononic–dielectric resonance can provide an important opportunity to construct metamaterial arrays with subwavelength lattice parameter far exceeding that of plasmonic and dielectric Mie resonance metamaterials.

The proposed metamaterial consists of germanium disks arrays on 6H-SiC polar substrate (schematically illustrated in Figure 1a). Several arrays with different diameters of the discs were fabricated to demonstrate tunability of the metamaterial optical response on the proposed platform. Figure 1b shows an example of the experimental structure visualized using the scanning electron microscope (SEM). The relative dimensions of germanium resonators here correspond to the volume of the single disk metamolecule on the order of  $\lambda_0^3/10^4$ . The unit cells of the metamaterial are arranged in a hexagonal lattice and the gaps between adjacent germanium discs are fixed at 200 nm. The thickness ( $h$ ) of the disks equals to 120 nm and the diameters ( $D$ ) vary between different experimentally fabricated arrays from 300 to 2000 nm. The fabrication of the structures was done by chemical-etching-free nanopatterning technique and preserves the intrinsic quality of the polar crystal substrate.<sup>[10]</sup> The designed patterns, here, are defined using electron beam lithography. The layer of germanium is subsequently evaporated onto the developed e-beam resist, and the final experimental structures are revealed by lift-off.


At first, we study the field enhancement and the impact of germanium layer thickness on mid-IR optical response of the proposed metamaterial using numerical simulations. Figure 1c,d shows the calculated electric field distribution

Dr. B. Qiang, Dr. A. M. Dubrovkin, Dr. H. N. S. Krishnamoorthy, Prof. N. I. Zheludev, Prof. Q. J. Wang  
Centre for Disruptive Photonic Technologies  
TPI  
SPMS  
Nanyang Technological University  
Singapore 637371, Singapore  
E-mail: dubrovkin@ntu.edu.sg; niz@orc.soton.ac.uk; qjwang@ntu.edu.sg

Dr. B. Qiang, Prof. Q. J. Wang  
Centre for OptoElectronics and Biophotonics  
School of Electrical and Electronic Engineering  
Nanyang Technological University  
Singapore 639798, Singapore

Dr. Q. Wang  
Institute of Materials Research and Engineering  
Agency for Science, Technology and Research (A\*STAR)  
2 Fusionopolis Way, Innovis #08-03, Singapore 138634, Singapore

Prof. N. I. Zheludev  
Optoelectronics Research Centre and Centre for Photonic Metamaterials  
University of Southampton  
Southampton SO17 1BJ, UK

 The ORCID identification number(s) for the author(s) of this article can be found under <https://doi.org/10.1002/adom.202001652>.

DOI: 10.1002/adom.202001652

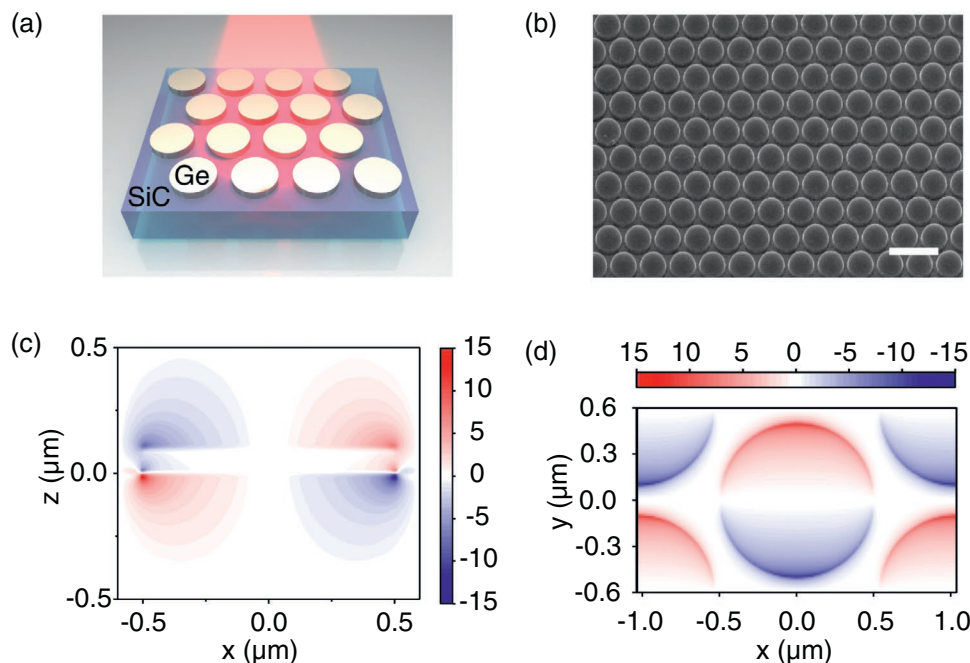


**Figure 1.** a) Schematics of the hybrid phononic–dielectric metamaterial representing array of Ge disks on SiC substrate. b) SEM image of the fabricated metamaterial with Ge disk thickness of 120 nm and diameter of 1  $\mu\text{m}$ , recorder at 52° tilting angle of the sample. The scale bar is 2  $\mu\text{m}$ . c,d) Simulated electric field enhancement of  $\text{Re}(E_z)$  along  $x$ - $z$  and  $x$ - $y$  directions, respectively, calculated at  $\lambda = 11.2 \mu\text{m}$  for the nominal geometry of the fabricated structure. The color bar represents calculated electric field normalized by the electric field of the incident light.

( $\text{Re}(E_z)$ ) in the metamaterial ( $D = 1 \mu\text{m}$ ) tuned into the resonance at  $\lambda = 11.2 \mu\text{m}$ . As can be seen from Figure 1d, the appeared resonance is dipolar in nature and provides electric field enhancement as large as 15, compared to the electric field of the incident light. **Figure 2a** shows the simulated reflection spectra of hybrid metamaterials when  $D$  is fixed (to 1  $\mu\text{m}$ ) and the height  $h$  is gradually varied from 20 to 200 nm. The reflection spectra are normalized to the reflection spectrum of a bare SiC substrate. The simulation results showed that strong resonance is observed for almost all the thicknesses at the wavelength around 11  $\mu\text{m}$ . As for 6H-SiC the reflectivity is approximately unity in this wavelength range, a dip in reflection spectra indicates the amount of light been absorbed by

the structures. For instance, the 20 nm thick germanium disk arrays on SiC could lead to the absorption of about 30%. When the thickness of the Ge disk increases, the resonance redshifts and the absorption increases. In particular, when the thickness reaches 120 nm, almost all incident light is absorbed and the metamaterial performs as a perfect absorber. Strong absorption in the infrared spectral range is important in many practical applications such as modulators,<sup>[11]</sup> phase arrays,<sup>[12]</sup> thermal radiation management,<sup>[13–17]</sup> and thermal cooling.<sup>[18]</sup> The presented simulation results demonstrate the potential of the proposed hybrid metamaterials for building high-density mid-IR resonant devices based on planar germanium patterns of nanometric thickness on silicon carbide.

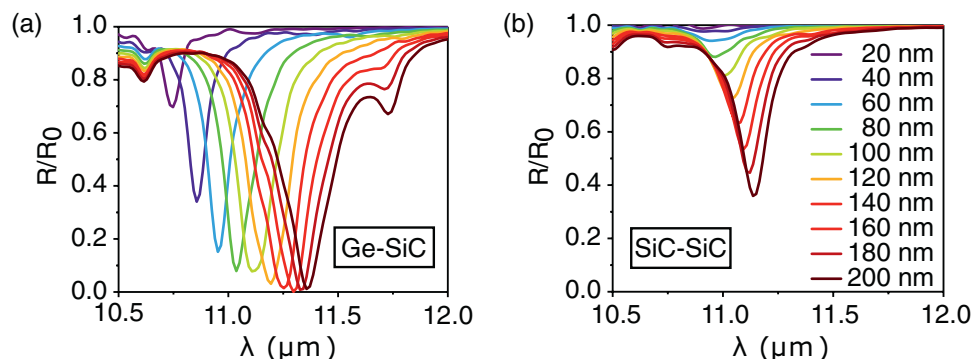


**Figure 2.** Simulated reflection spectra of phonon-polaritonic metamaterials. a) Calculations for Ge disks of 1  $\mu\text{m}$  diameter and varying thickness on SiC substrate. The used thicknesses of Ge disks are in the range from 20 to 200 nm and labeled by color according to the same legend as given in panel (b). b) Calculations for SiC disks of 1  $\mu\text{m}$  diameter and varying thickness on SiC for comparison. The spectra are normalized to the reflection spectrum of bare SiC substrate.

As bare phononic silicon carbide has been actively employed for building mid-IR devices,<sup>[19,20]</sup> we further compare the discussed hybrid phononic–dielectric metamaterial performance with reference structures consisting of pure silicon carbide arrays of similar design and height profiles (i.e., Ge is replaced with SiC). In simulations, all the structure sizes such as diameters, lattice spacings, and heights are kept the same as those used in the previous case. The smaller absorption in the reflection spectra (Figure 2b), unambiguously indicates that such monolithic structures resonate much weaker than the hybrid phononic–dielectric metamaterials (Figure 2a). In particular, the 20 nm thick SiC disks array does not show any observable absorption. When the thickness increases to 120 nm, the absorption increases to about 25%. The 200 nm thick metamaterial absorbs only up to 60% of the total incident light.

The difference in the absorption efficiency can be explained by the different underlying mechanisms of the resonances on SiC, with and without germanium layer. Conceptually, each bare SiC-disk metamaterial in Figure 2b can be regarded as an array of surface phonon-polaritonic cavities. The thickness of the disks is much smaller than the decay length of the evanescent wave supported by bare SiC–air interface. The disk edges only cause small perturbations to the polaritonic field, which therefore escapes from the cavity easily. Such inefficient confinement of the polaritonic field on monolithic SiC makes the absorption negligible on low-profile structures. For instance, in previous studies on bare silicon carbide, strong surface

phonon-polariton resonances were usually achieved by dry etching of SiC to as deep as 1  $\mu\text{m}$ /sub- $\mu\text{m}$  profiles.<sup>[16,19,21–26]</sup> The hybrid phononic–dielectric metamaterial, on the other hand, is based on composite resonant cavities supporting highly confined type of phononic surface waves.<sup>[27–29]</sup> Such a configuration provides a significant reduction of the decay length of the interface evanescent wave in air, enabling efficient trapping of the polaritonic field in phononic–dielectric devices.

Next, we investigate the dependence of the metamaterial resonance on the diameter of germanium disk. Figure 3a,b shows full-wave simulations and experimentally measured reflection spectra, respectively. The disk diameters here are 300, 500, 1000, 1500, and 2000 nm. All results are normalized to the reflection spectrum of bare SiC substrate. The simulations show that perfect absorption can be achieved when  $D$  is larger than 1  $\mu\text{m}$ . The resonant wavelength blueshifts when the size of the metamolecule increases. Such trend can be explained by anomalous dispersion<sup>[27,28]</sup> supported by the highly confined surface phonon-polaritons on hybrid phononic–dielectric interfaces. In the resonant region of the experimental metamaterial structures, the wavenumber of the polaritonic mode increases upon increasing the free space excitation wavelength (Figure 3c). The extracted positions of the reflection dips in the experimental data agree well with predicted resonating wavelengths in simulations (Figure 3d). The highest  $Q$ -factor achieved experimentally is  $\approx 54$ , which is higher than most of the noble metal<sup>[30–32]</sup> and graphene-based plasmonic metamaterials.<sup>[33,34]</sup> We note

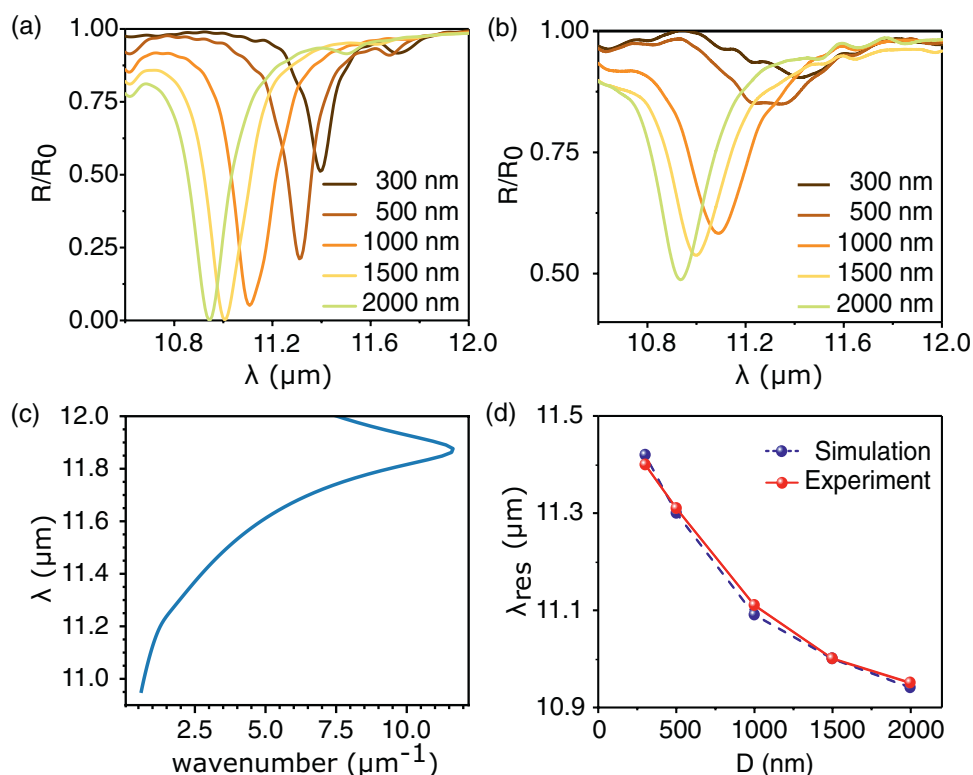


**Figure 3.** Dependence of the hybrid phononic–dielectric metamaterial resonance on the germanium disk diameter. a,b) Simulated and measured normalized reflection spectra of the SiC–Ge metamaterial, respectively. The used diameters of Ge disks are 300, 500, 1000, 1500, and 2000 nm, and the thickness of Ge is 120 nm. c) Dispersion of highly confined surface phonon-polariton mode calculated based on the rigorous equation (in the Supporting Information of ref. [28]) for 120 nm thick Ge on SiC. d) Extracted resonant wavelengths corresponding to the data in panels (a) and (b).

that the difference between the experimental  $Q$ -factors and the strength of the resonances compared to simulations could be attributed to imperfections of the device fabrication. For instance, a change in germanium edge shape and roughness may induce an extra scattering from the disks. Such effects are more pronounced at smaller structures, and could be potentially improved by optimizing the lithographic process.

As a proof-of-concept demonstration of potential applications, we test the performance of fabricated Ge-SiC metamaterials as refractive index sensors. As an analyte here, a layer of poly(methyl methacrylate) (PMMA) 950k was spin-coated at 6000 rpm on top of the hybrid metamaterial surfaces and baked at 160 °C for 5 min. The thickness of the PMMA layer is estimated to be 150 nm based on the spin curve, and the refractive index is  $\approx 1.5$  at the relevant wavelength regime.<sup>[35]</sup> Figure 4 shows the reflection spectrum before and after coating of the PMMA layer. A significant shift of the resonant wavelength can be observed after PMMA coating for all the three metamaterials used for demonstration. Metamaterials with diameter 2000 nm showed largest spectrum shift of 140 nm, which corresponds to a sensitivity of 280 nm RIU<sup>-1</sup>. The full width at half maximum (FWHM) of the dipolar resonance is  $\approx 200$  nm, therefore the figure of merit for the index sensing (i.e., the sensitivity divided to FWHM) is about 1.4 RIU<sup>-1</sup>.

In summary, we have experimentally demonstrated a new type of complementary metal–oxide–semiconductor (CMOS)-compatible metamaterials for mid-IR densely integrated devices and systematically investigated its electromagnetic properties. These metamaterials are based on surface phonon-polariton resonators (Ge on SiC) of deep subwavelength sizes and planar design principles, enabling homogeneous medium with tunable optical response. As such metamaterials feature higher quality factors than in conventional plasmonics, we foresee its potential for refractive index sensing or surface-enhanced infrared absorption applications. We also note that although some of 2D hyperbolic phononic materials (such as boron nitride<sup>[36]</sup>) may also share the same advantages, the concept of hybrid metamaterial demonstrated here can be directly transferred to a number of technologically important phononic

substrates (such as sapphire, quartz, etc.) and dielectric coatings. The large degree of freedom in material choices provides much wider working wavelength range enabling flexibility in the designs of potential infrared devices.

## Experimental Section

**Fabrication of Germanium-on-Carborundum Metamaterial:** The metamaterials arrays ( $50 \times 50 \mu\text{m}$  in size) were fabricated by electron beam lithography technique. A layer of PMMA (MicroChem A4 950k) was spin-coated onto an epi-ready surface of 6H-SiC substrate at 4000 rpm for 45 s. The resist was post-baked at 160 °C for 5 min. The patterns were transferred onto the resist using Helios NanoLab DualBeam system with 30 kV accelerating voltage and 25 pA current. The development of the patterns was performed using methyl isobutyl ketone/isopropyl alcohol (MIBK/IPA 1:3, MicroChem) solution for 45 s. The germanium film was thermally evaporated on the patterned resist using UNIVEX 250 system at  $0.2 \text{ \AA s}^{-1}$  deposition rate and subsequently lifted off in acetone following by rinsing with IPA.

**Numerical Simulations:** Numerical simulations were performed using commercial software (Lumerical FDTD). The dimension of the structure is defined in the text. The boundary conditions in  $x$ - and  $y$ -directions are “Periodic” and “PML” in  $z$ -direction. A plane wave source was incident onto the metamaterials, and the reflection spectra were recorded by placing a power monitor behind the light source. Simulated reflection curves in Figure 2 were generated at normal incidence while those in Figure 3a were generated in oblique configuration to match experimental conditions.

**Infrared Spectroscopy:** The reflection spectra of the fabricated metamaterials were measured using a Fourier transform infrared spectrometer (Bruker Vertex 80v) equipped with a confocal microscope (Hyperion 1000). The detector used is a liquid-nitrogen-cooled mercury cadmium telluride detector. The aperture of the microscope is set to be  $50 \mu\text{m} \times 50 \mu\text{m}$  for all measurements. Positions of the reflection dips in the recorded spectra were extracted using fitting of the experimental data (Figure S1, Supporting Information). For the sensing experiment, the additional spectra were recorded after spin-coating of PMMA onto the fabricated metamaterials.

## Supporting Information

Supporting Information is available from the Wiley Online Library or from the author.

## Acknowledgements

B.Q. and A.M.D. contributed equally to this work. This research was supported by the Singapore Ministry of Education (Academic Research Fund MOE2016-T3-1-006 (S) and Grant No. MOE2018-T2-1-176), by Advanced Manufacturing and Engineering Grant from the Agency for Science, Technology and Research (A\*STAR) (Award No. A18A7b0058), by the National Research Foundation Singapore programs NRF-CRP18-2017-02 and NRF-CRP19-2017-01, and by the UK Engineering and Physical Sciences Research Council (Grant No. EP/M009122/1).

## Conflict of Interest

The authors declare no conflict of interest.

## Data Availability Statement

Following a period of embargo, the data from this paper will be available from the University of Southampton repository: <https://doi.org/10.5258/SOTON/D1673>.

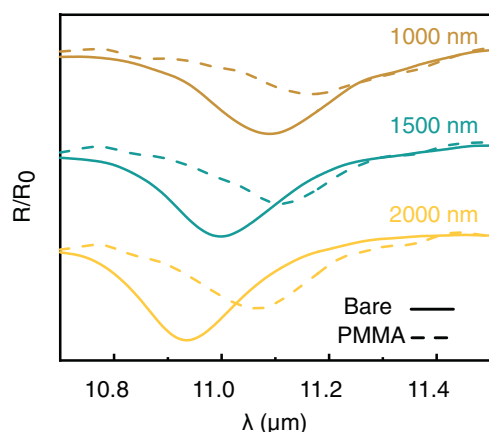


**Figure 4.** Refractive index sensing using hybrid phononic–dielectric metamaterials. The plotted curves of normalized reflection spectra are shifted along the vertical axis for better visibility; the diameters of Ge disks for each of the fabricated metamaterials are highlighted next to the corresponding curve.

## Keywords

germanium, metamaterials, mid-IR resonance, silicon carbide, surface phonon-polaritons

Received: September 23, 2020

Revised: November 29, 2020

Published online: December 18, 2020

- 
- [1] J. B. Pendry, A. J. Holden, D. J. Robbins, W. J. Stewart, *IEEE Trans. Microw. Theory Tech.* **1999**, *47*, 2075.
- [2] J. Valentine, S. Zhang, T. Zentgraf, E. Ulin-Avila, D. A. Genov, G. Bartal, X. Zhang, *Nature* **2008**, *455*, 376.
- [3] V. A. Fedotov, P. L. Mladyonov, S. L. Prosvirnin, A. V. Rogacheva, Y. Chen, N. I. Zheludev, *Phys. Rev. Lett.* **2006**, *97*, 167401.
- [4] T. Kaelberer, V. A. Fedotov, N. Papasimakis, D. P. Tsai, N. I. Zheludev, *Science* **2010**, *330*, 1510.
- [5] C. Kurter, A. P. Zhuravel, J. Abrahams, C. L. Bennett, A. V. Ustinov, S. M. Anlage, *IEEE Trans. Appl. Supercond.* **2011**, *21*, 709.
- [6] A. S. Averkin, A. Karpov, A. P. Zhuravel, L. V. Filippenko, V. P. Koshelets, S. M. Anlage, A. V. Ustinov, *IEEE Trans. Appl. Supercond.* **2017**, *27*, 1502204.
- [7] T. Koschny, M. Kafesaki, E. N. Economou, C. M. Soukoulis, *Phys. Rev. Lett.* **2004**, *93*, 107402.
- [8] Y. Wu, Y. Lai, Z.-Q. Zhang, *Phys. Rev. B* **2007**, *76*, 205313.
- [9] R. Liu, T. J. Cui, D. Huang, B. Zhao, D. R. Smith, *Phys. Rev. E* **2007**, *76*, 26606.
- [10] B. Qiang, A. M. Dubrovkin, H. N. S. Krishnamoorthy, Q. Wang, C. Soci, Y. Zhang, J. Teng, Q. J. Wang, *Adv. Photonics* **2019**, *1*, 026001.
- [11] S. Kim, M. S. Jang, V. W. Brar, K. W. Mauser, L. Kim, H. A. Atwater, *Nano Lett.* **2018**, *18*, 971.
- [12] M. C. Sherrott, P. W. C. Hon, K. T. Fountaine, J. C. Garcia, S. M. Ponti, V. W. Brar, L. A. Sweatlock, H. A. Atwater, *Nano Lett.* **2017**, *17*, 3027.
- [13] J.-J. Greffet, R. Carminati, K. Joulain, J.-P. Mulet, S. Mainguy, Y. Chen, *Nature* **2002**, *416*, 61.
- [14] J. A. Schuller, T. Taubner, M. L. Brongersma, *Nat. Photonics* **2009**, *3*, 658.
- [15] Y. Zhai, Y. Ma, S. N. David, D. Zhao, R. Lou, G. Tan, R. Yang, X. Yin, *Science* **2017**, *355*, 1062.
- [16] T. Wang, P. Li, D. N. Chigrin, A. J. Giles, F. J. Bezares, O. J. Glembocki, J. D. Caldwell, T. Taubner, *ACS Photonics* **2017**, *4*, 1753.
- [17] G. Lu, J. R. Nolen, T. G. Folland, M. J. Tadjer, D. G. Walker, J. D. Caldwell, *ACS Omega* **2020**, *5*, 10900.
- [18] A. Howes, J. R. Nolen, J. D. Caldwell, J. Valentine, *Adv. Opt. Mater.* **2020**, *8*, 1901470.
- [19] J. D. Caldwell, O. J. Glembocki, Y. Francescato, N. Sharac, V. Giannini, F. J. Bezares, J. P. Long, J. C. Owrutsky, I. Vurgaftman, J. G. Tischler, V. D. Wheeler, N. D. Bassim, L. M. Shirey, R. Kasica, S. A. Maier, *Nano Lett.* **2013**, *13*, 3690.
- [20] J. D. Caldwell, L. Lindsay, V. Giannini, I. Vurgaftman, T. L. Reinecke, S. A. Maier, O. J. Glembocki, *Nanophotonics* **2015**, *4*, 44.
- [21] Y. Chen, Y. Francescato, J. D. Caldwell, V. Giannini, T. W. W. Maß, O. J. Glembocki, F. J. Bezares, T. Taubner, R. Kasica, M. Hong, S. A. Maier, *ACS Photonics* **2014**, *1*, 718.
- [22] C. T. Ellis, J. G. Tischler, O. J. Glembocki, F. J. Bezares, A. J. Giles, R. Kasica, L. Shirey, J. C. Owrutsky, D. N. Chigrin, J. D. Caldwell, *Sci. Rep.* **2016**, *6*, 32959.
- [23] A. D. Dunkelberger, C. T. Ellis, D. C. Ratchford, A. J. Giles, M. Kim, C. S. Kim, B. T. Spann, I. Vurgaftman, J. G. Tischler, J. P. Long, O. J. Glembocki, J. C. Owrutsky, J. D. Caldwell, *Nat. Photonics* **2018**, *12*, 50.
- [24] R. Berte, C. R. Gubbin, V. D. Wheeler, A. J. Giles, V. Giannini, S. A. Maier, S. De Liberato, J. D. Caldwell, *ACS Photonics* **2018**, *5*, 2807.
- [25] C. R. Gubbin, R. Berte, M. A. Meeker, A. J. Giles, C. T. Ellis, J. G. Tischler, V. D. Wheeler, S. A. Maier, J. D. Caldwell, S. De Liberato, *Nat. Commun.* **2019**, *10*, 1682.
- [26] R. Kiessling, Y. Tong, A. J. Giles, S. Gewinner, W. Schöllkopf, J. D. Caldwell, M. Wolf, A. Paarmann, *ACS Photonics* **2019**, *6*, 3017.
- [27] P. Li, X. Yang, T. W. W. Maß, J. Hanss, M. Lewin, A.-K. U. Michel, M. Wuttig, T. Taubner, *Nat. Mater.* **2016**, *15*, 870.
- [28] A. M. Dubrovkin, B. Qiang, H. N. S. Krishnamoorthy, N. I. Zheludev, Q. J. Wang, *Nat. Commun.* **2018**, *9*, 1762.
- [29] A. M. Dubrovkin, B. Qiang, T. Salim, D. Nam, N. I. Zheludev, Q. J. Wang, *Nat. Commun.* **2020**, *11*, 1863.
- [30] X. Liu, T. Tyler, T. Starr, A. F. Starr, N. M. Jokerst, W. J. Padilla, *Phys. Rev. Lett.* **2011**, *107*, 045901.
- [31] A. Lochbaum, Y. Fedoryshyn, A. Dorodnyy, U. Koch, C. Hafner, J. Leuthold, *ACS Photonics* **2017**, *4*, 1371.
- [32] A. Tittl, A. K. U. Michel, M. Schäferling, X. Yin, B. Gholipour, L. Cui, M. Wuttig, T. Taubner, F. Neubrech, H. Giessen, *Adv. Mater.* **2015**, *27*, 4597.
- [33] H. Yan, T. Low, W. Zhu, Y. Wu, M. Freitag, X. Li, F. Guinea, P. Avouris, F. Xia, *Nat. Photonics* **2013**, *7*, 394.
- [34] D. Rodrigo, O. Limaj, D. Janner, D. Etezadi, F. J. G. De Abajo, V. Pruneri, H. Altug, *Science* **2015**, *349*, 165.
- [35] S. Jitian, I. Bratu, *AIP Conf. Proc.* **2012**, *1425*, 26.
- [36] J. D. Caldwell, A. V. Kretinin, Y. Chen, V. Giannini, M. M. Fogler, Y. Francescato, C. T. Ellis, J. G. Tischler, C. R. Woods, A. J. Giles, M. Hong, K. Watanabe, T. Taniguchi, S. A. Maier, K. S. Novoselov, *Nat. Commun.* **2014**, *5*, 5221.